Vortex State and Field-Angle Resolved Specific Heat Oscillation for $H \parallel ab$ in d-Wave Superconductors

Masayuki Hiragi, Kenta M. Suzuki [*], Masanori Ichioka [†], Kazushige Machida [‡]

Department of Physics, Okayama University, Okayama 700-8530, Japan

When magnetic field is applied parallel to the *ab* plane in $d_{x^2-y^2}$-wave superconductors, the transition of stable vortex lattice structure, spatial structure of local density of states, and specific heat oscillation by rotation of magnetic field orientation are investigated by quantitative calculations based on the selfconsistent Eilenberger theory. We estimate how the vortex state changes depending on the relative angle between the node-direction of the superconducting gap and magnetic field orientation. To reproduce the sign-change of specific heat oscillation observed in CeCoIn$_5$, our study is done by including strong paramagnetic effect. The quantitative theoretical calculations give decisive information to analyze the experimental data on the field-angle dependence, and establish the angle-resolved specific heat experiment as a spectroscopic means to identify the node-position of the superconducting gap.

KEYWORDS: vortex state under parallel field, paramagnetic effect, specific heat oscillation, Eilenberger theory

1. Introduction

In unconventional superconductors such as heavy fermion superconductors, high-T_c cuprate superconductors, organic superconductors, the pairing mechanism may not be conventional electron-phonon interaction. The Cooper pairs are formed by exotic pairing mechanism coming from the strong electron-electron interaction, and possibly the pairing symmetry is *p*-, *d*-, or *f*-wave, other than full gap *s*-wave. Thus, the pairing function has sign change on the Fermi surface, resulting in nodes of the superconducting gap. To clarify the mechanism of unconventional superconductors, it is important to identify the pairing symmetry of the Cooper pairs.

Experimentally, existence of the node can be detected by the power-law dependence of physical quantities as a function of temperature *T*. For example, the specific heat $C \propto T^2$ ($\propto T^3$) and nuclear spin relaxation rate $T_1^{-1} \propto T^3$ ($\propto T^5$) for line (point) node of superconducting gap, instead of exponential *T*-dependence for full gap *s*-wave pairing.[1] This comes from the power-law of the density of states (DOS) $N(E) \propto E$ ($\propto E^2$) for the line (point) nodes of the gap function.

The position of the node on the Fermi surface can be identified by the phase-sensitive experimental methods such as corner junction[2,3] and Andreev surface bound states.[4] For these experiments, we need delicate fabrication techniques to set up a good junction. Another method to detect the node position is magnetic field orientation-sensitive experiments for physical quantities of bulk measurement.[5–7] There, by rotating magnetic field orientation, we try to identify the position of the nodes from the change of physical quantities, such as specific heat,[8–15] and thermal conductivity,[16] depending on the relative angle between magnetic field orientation and the node-direction. These quantities under magnetic fields reflect electronic excitation in the vortex states. For reliable analysis of the experimental data and establishing those methods as a spectroscopic means of the gap node position determination, these electronic behaviors have to be confirmed by
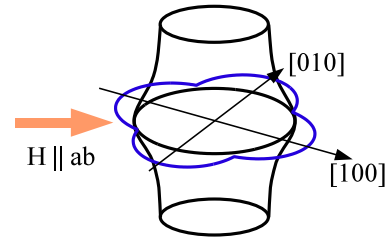

Fig. 1. (Color online) Schematic configuration of magnetic field and $d_{x^2-y^2}$-wave superconducting gap on rippled cylindrical Fermi surface. We discuss the case when magnetic field is applied parallel to the *ab* plane.

quantitative estimate of theoretical calculation in the vortex states. In this paper, we study the vortex states and the field-angle sensitive specific heat under magnetic fields parallel to the *ab* plane, related to the pairing gap in a heavy fermion superconductor CeCoIn$_5$. For CeCoIn$_5$, there were controversial discussions as for the pairing symmetry between $d_{x^2-y^2}$-wave and d_{xy}-wave.[14]

We consider the case when the magnetic field orientation is rotated within the *ab*-plane, and the Fermi-surface is quasi-two dimensional (Q2D), as shown in Fig. 1. In this *ab* plane magnetic field configuration, we calculate the vortex structure selfconsistently with electronic states by quasiclassical Eilenberger theory. The selfconsistent calculation is necessary for quantitative estimate of physical quantities, because we have to determine the vortex core radius accurately. By these calculations, we investigate (1) the stable vortex lattice structure, (2) the local density of states (LDOS) of electrons in the vortex lattice state, and (3) the amplitude of specific heat oscillation under field rotation. We discuss their differences between magnetic field orientations **H** ∥ node and **H** ∥ antinode. In $d_{x^2-y^2}$-wave pairing, [1, 1, 0] is node-direction, and [1, 0, 0] is antinode-direction.

(1) The configuration of the vortex lattice reflects the anisotropy of superconductivity such as *d*-wave pairing. When **H** ∥ *c*, due to the fourfold symmetry on the Fermi sur-

---

[*] E-mail address: kenta@mp.okayama-u.ac.jp

[†] E-mail address: oka@mp.okayama-u.ac.jp

[‡] E-mail address: machida@mp.okayama-u.ac.jp

face, triangular vortex lattice at low fields becomes the deformed lattice, accompanied by a first order transition of lattice orientation change, and finally reduces to a square vortex lattice.[17] When $\mathbf{H} \parallel ab$, effects of anisotropic superconductivity on the vortex lattice configuration is not enough clarified. Thus, in this field direction, we discuss the transition between two possible vortex lattice configuration, depending T or field orientation within the ab plane.

(2) In the LDOS when $\mathbf{H} \parallel c$, the zero-energy electronic states around vortex show star-shape spatial pattern, reflecting the anisotropy of the pairing gap function. The low-energy states extend from the vortex core toward the node (or minimum gap) directions.[18, 19] In this paper we discuss the LDOS around vortices when $\mathbf{H} \parallel ab$, both for $\mathbf{H} \parallel$ node and $\mathbf{H} \parallel$ antinode. The LDOS structure mainly reflects properties of Q2D Fermi surface.

(3) Since low temperature specific heat is proportional to zero-energy DOS $N(E = 0)$, the oscillation of $N(E = 0)$ by rotating magnetic field orientation was estimated by Doppler shift method[5] and microscopical Eilenberger theory.[6, 7] While the Doppler shift method[20] is a handy estimate to intuitively understand the oscillation, for quantitative comparison with experimental data, we have to carefully evaluate the oscillation amplitude by quantitatively reliable theoretical method such as Eilenberger theory, since the oscillation amplitude is in the order of a few percent of the total specific heat value.

In the early stage of the specific heat experiment for CeCoIn$_5$,[9] the sign of the oscillation was not consistent with the $d_{x^2-y^2}$-wave pairing. The $d_{x^2-y^2}$-wave pairing was suggested by some experiments, such as the oscillation of thermal conductivity by rotating magnetic fields,[16] flux line lattice transformation,[17, 21–23] point-contact Andreev reflection,[24] and spin resonance.[25, 26] In order to settle the contradiction between the $d_{x^2-y^2}$-wave pairing and the specific heat oscillation, the possibility of the sign change as a function of T was proposed.[27, 28] Since the sign of the oscillation is changed at intermediate T range, the sign can be opposite to that expected at low T. The previous work by Eilenberger theory for the sign change was done by the Pesch approximation,[27] where the spatial dependence of the quasiclassical Green's function g is neglected, replacing g to the spatial average of g. In this paper, we quantitatively calculate the amplitude and sign of the specific heat oscillation by Eilenberger theory fully selfconsistently without using Pesch approximation. Extending this method further, we evaluate the contribution of strong paramagnetic effect and anisotropic Fermi surface velocity on the oscillation. The anisotropic Fermi velocity is another key factor other than the anisotropic superconducting gap, when we consider the vortex structure in anisotropic superconductors. The sign change of the specific heat oscillation at low T and low H has been recently observed in CeCoIn$_5$, which confirms $d_{x^2-y^2}$-wave pairing.[15] Part of the results in this paper was reported in ref. 15 as theoretical analysis for the experiment.

It is noted that the strong paramagnetic effect is important and indispensable when we discuss the vortex states in CeCoIn$_5$. The paramagnetic effect comes from mismatched Fermi surfaces of up- and down-spin electrons due to the large Zeeman splitting. At higher fields in the case of strong paramagnetic effect, the upper critical field H_{c2} changes to the first order phase transition[16, 29, 30] and new Fulde-Ferrell-Larkin-Ovchinnikov (FFLO) state may appear.[31–40] Even in the vortex states at low field before entering to the FFLO state, the strong paramagnetic effects induces anomalous behavior of physical quantities,[30, 41–43] including field dependence of flux line lattice form factor.[21, 44] Therefore, we consider contributions of the strong paramagnetic effect in the studies of items (1)-(3).

After giving our formulation of quasiclassical theory in the presence of the paramagnetic effect in §2, we study the stable vortex lattice configuration in §3 and the zero-energy LDOS structure in §4 for two field orientations $\mathbf{H} \parallel$ node and $\mathbf{H} \parallel$ antinode, when $\mathbf{H} \parallel ab$ in the $d_{x^2-y^2}$-wave pairing. In §5, we estimate the H- and T-dependences of amplitude and sign of specific heat oscillation by rotating the magnetic field orientation within the ab-plane, in the presence of strong paramagnetic effect and anisotropic Fermi velocity in addition to the d-wave pairing. The last section is devoted to summary and discussions.

2. Formulation by Selfconsistent Quasiclassical Theory

We calculate the spatial structure of the vortex lattice state by quasiclassical Eilenberger theory in the clean limit.[45–48] The quasiclassical theory is quantitatively valid when $\xi \gg 1/k_F$ (k_F is the Fermi wave number, and ξ is the superconducting coherence length), which is satisfied in most of superconductors in solid states. When the paramagnetic effects are discussed, we include the Zeeman term $\mu_B B(\mathbf{r})$, where $B(\mathbf{r})$ is the flux density of the internal field and μ_B is a renormalized Bohr magneton.[43, 49–51] The quasiclassical Green's functions $g(\omega_n + i\mu B, \mathbf{k}, \mathbf{r})$, $f(\omega_n + i\mu B, \mathbf{k}, \mathbf{r})$, and $f^\dagger(\omega_n + i\mu B, \mathbf{k}, \mathbf{r})$ are calculated in the vortex lattice state by the Eilenberger equation

$$\{\omega_n + i\mu B + \tilde{\mathbf{v}} \cdot (\nabla + i\mathbf{A})\} f = \Delta\phi g,$$

$$\{\omega_n + i\mu B - \tilde{\mathbf{v}} \cdot (\nabla - i\mathbf{A})\} f^\dagger = \Delta^*\phi^* g, \qquad (1)$$

where $g = (1 - ff^\dagger)^{1/2}$, $\text{Re}\, g > 0$, $\tilde{\mathbf{v}} = \mathbf{v}/v_{F0}$, and $\mu = \mu_B B_0/\pi k_B T_c$. $\mathbf{k} = (k_a, k_b, k_c)$ is the relative momentum of the Cooper pair, and $\mathbf{r}$ is the center-of-mass coordinate of the pair. We set the pairing function $\phi(\mathbf{k}) = \phi_{x^2-y^2}(\mathbf{k}) = \sqrt{2}(k_a^2 - k_b^2)/(k_a^2 + k_b^2)$ in $d_{x^2-y^2}$-wave pairing, and magnetic fields are applied to $[1, 0, 0]$ or $[1, 1, 0]$ directions in the crystal coordinate. For example, when a magnetic field is applied to $[1, 0, 0]$ direction, the coordinate (x, y, z) for the vortex structure corresponds to (b, c, a) of the crystal coordinate. In the case of d_{xy}-wave pairing $\phi(\mathbf{k}) = \phi_{xy}(\mathbf{k}) = 2\sqrt{2}k_ak_b/(k_a^2 + k_b^2)$, the results for $[1, 0, 0]$ and $[1, 1, 0]$ field directions are exchanged.

In our calculation, length, temperature, Fermi velocity, magnetic field and vector potential are, respectively, scaled by R_0, T_c, $\bar{v}_F$, B_0 and B_0R_0. Here, $R_0 = \hbar\bar{v}_F/2\pi k_B T_c$, $B_0 = \phi_0/2\pi R_0^2$ with the flux quantum ϕ_0, and $\bar{v}_F = \langle v_F^2 \rangle_{\mathbf{k}}^{1/2}$ is an averaged Fermi velocity on the Fermi surface. $\langle \cdots \rangle_{\mathbf{k}}$ indicates the Fermi surface average. The energy E, pair potential Δ and Matsubara frequency ω_l are in unit of $\pi k_B T_c$. As a model of the Fermi surface, for simplicity, we use a Q2D Fermi surface with rippled cylinder-shape, and the Fermi velocity is given by

$$\mathbf{v}_F = (v_a, v_b, v_c) \propto (\tilde{v}\cos\theta_k, \tilde{v}\sin\theta_k, \tilde{v}_z\sin k_c) \qquad (2)$$

at the Fermi surface $\mathbf{k}_F = (k_a, k_b, k_c) \propto (k_{F0}\cos\theta_k, k_{F0}\sin\theta_k, k_c)$ with $-\pi \le \theta_k \le \pi$ and $-\pi \le k_c \le \pi$.[52] To include the Fermi velocity anisotropy, we use $\tilde{v} = 1 + \beta\cos 4\theta_k$. In our calculation except for last part, $\beta = 0$ since we mainly consider the case when the Fermi velocity is isotropic in the *ab*-plane. In our work, we set $\tilde{v}_z = 0.5$, so that the anisotropy ratio

$$\gamma = \frac{\xi_c}{\xi_{ab}} \sim \frac{\langle v_c^2 \rangle_{\mathbf{k}}^{1/2}}{\langle v_a^2 \rangle_{\mathbf{k}}^{1/2}} \sim 0.5, \tag{3}$$

as in CeCoIn$_5$.

When magnetic fields are applied to the z axis of the vortex coordinate, the vector potential $\mathbf{A}(\mathbf{r}) = \frac{1}{2}\mathbf{H} \times \mathbf{r} + \mathbf{a}(\mathbf{r})$ in the symmetric gauge, where $\mathbf{H} = (0, 0, H)$ is a uniform flux density and $\mathbf{a}(\mathbf{r})$ is related to the internal field $\mathbf{B}(\mathbf{r}) = \mathbf{H} + \nabla \times \mathbf{a}(\mathbf{r})$. The unit cell of the vortex lattice is given by $\mathbf{r} = s_1(\mathbf{u}_1 - \mathbf{u}_2) + s_2\mathbf{u}_2$ with $-0.5 \le s_i \le 0.5$ (i=1, 2), $\mathbf{u}_1 = (a_x, 0, 0)$, $\mathbf{u}_2 = (a_x/2, a_y, 0)$ and $a_x a_y B = \phi_0$.

As for selfconsistent conditions, the pair potential is calculated by

$$\Delta(\mathbf{r}) = g_0 N_0 T \sum_{0 < \omega_n \le \omega_{\mathrm{cut}}} \left\langle \phi^*(\mathbf{k})\left(f + f^{\dagger *}\right)\right\rangle_{\mathbf{k}} \tag{4}$$

with $(g_0 N_0)^{-1} = \ln T + 2T \sum_{0 < \omega_n \le \omega_{\mathrm{cut}}} \omega_l^{-1}$. We use $\omega_{\mathrm{cut}} = 20 k_B T_c$. The vector potential for the internal magnetic field is selfconsistently determined by

$$\nabla \times (\nabla \times \mathbf{A}) = \nabla \times \mathbf{M}_{\mathrm{para}}(\mathbf{r}) - \frac{2T}{\kappa^2} \sum_{0 < \omega_n} \langle \mathbf{v}_F \mathrm{Im} g \rangle_{\mathbf{k}}, \tag{5}$$

where we consider both the diamagnetic contribution of supercurrent in the last term and the contribution of the paramagnetic moment $\mathbf{M}_{\mathrm{para}}(\mathbf{r}) = (0, 0, M_{\mathrm{para}}(\mathbf{r}))$ with

$$M_{\mathrm{para}}(\mathbf{r}) = M_0 \left(\frac{B(\mathbf{r})}{H} - \frac{2T}{\mu H} \sum_{0 < \omega_n} \langle \mathrm{Im}\{g\} \rangle_{\mathbf{k}} \right). \tag{6}$$

The normal state paramagnetic moment $M_0 = (\mu/\kappa)^2 H$, $\kappa = B_0/\pi k_B T_c \sqrt{8\pi N_0}$ and N_0 is the DOS at the Fermi energy in the normal state. We set the Ginzburg-Landau parameter $\kappa = 89$ for this typical type-II superconductor. We solve eq. (1) and eqs. (4)-(6) alternately, and obtain selfconsistent solutions as in previous works,[43, 47, 48] under a given unit cell of the vortex lattice.

In Eilenberger theory, free energy is given by

$$F = \int_{\mathrm{unitcell}} d\mathbf{r}\Big\{\kappa^2|\mathbf{B}(\mathbf{r}) - \mathbf{H}|^2 - \mu^2|B(\mathbf{r})|^2$$

$$+ |\Delta(\mathbf{r})|^2 \Big(\ln T + 2T \sum_{0 < \omega_n < \omega_{\mathrm{cut}}} \omega_n^{-1}\Big)$$

$$- T \sum_{|\omega_n| < \omega_{\mathrm{cut}}} \langle I(\mathbf{r}, \mathbf{k}, \omega_n)\rangle\Big\} \tag{7}$$

with

$$I(\mathbf{r}, \mathbf{k}, \omega_n) = \Delta\phi f^{\dagger} + \Delta^*\phi^* f$$

$$+ \Big(g - \frac{\omega_n}{|\omega_n|}\Big)\Big\{\frac{1}{f}\big(\omega_n + i\mu B + \hat{\mathbf{v}} \cdot (\nabla + i\mathbf{A})\big) f$$

$$+ \frac{1}{f^{\dagger}}\big(\omega_n + i\mu B + \hat{\mathbf{v}} \cdot (\nabla - i\mathbf{A})\big) f^{\dagger}\Big\} \tag{8}$$
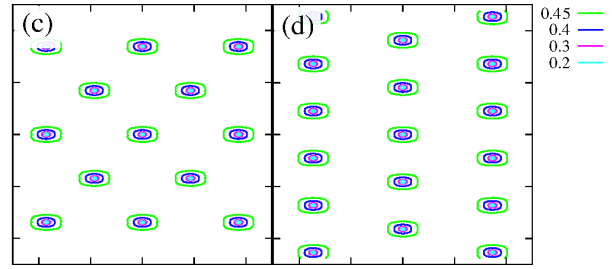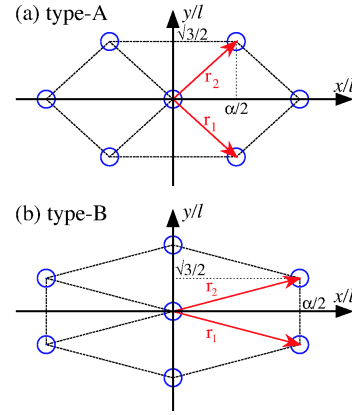

(a) type-A
(b) type-B

Fig. 2. (Color online) Possible stable vortex lattice configurations type-A (a) and type-B (b) when $\mathbf{H} \parallel ab$. (c) and (d) show the spatial structure of the pair potential $|\Delta(\mathbf{r})|$ in two vortex lattice configurations $\alpha = 1.9$ (a) and 6.6 (b) for $\mathbf{H} \parallel$ antinode. $\mu = 2$, $H/H_{c2} = 0.211$ and $T/T_c = 0.2$. Both (c) and (d) panels, the horizontal axis is [100] direction, and the vertical axis is [001] direction, and the view range is 25×25 in the Eilenberger length unit R_0.

in our dimensionless unit. Using eqs. (1) and (4), we obtain

$$F = \int_{\mathrm{unitcell}} d\mathbf{r}\Big\{\kappa^2|\mathbf{B}(\mathbf{r}) - \mathbf{H}|^2 - \mu^2|B(\mathbf{r})|^2$$

$$+ T \sum_{|\omega_n| < \omega_{\mathrm{cut}}} \mathrm{Re}\left\langle \frac{g-1}{g+1}(\Delta\phi f^{\dagger} + \Delta^*\phi^* f)\right\rangle\Big\}. \tag{9}$$

The entropy in the superconducting state, given by $S_s(T) = S_n(T) - \partial F/\partial T$, is obtained from eqs. (7) and (8) as

$$\frac{S_s(T)}{S_n(T_c)} = T - \frac{3}{2}\int_{\mathrm{unitcell}} d\mathbf{r}\Big\{$$

$$(\ln T + 2T \sum_{0 < \omega_n < \omega_{\mathrm{cut}}} \omega_n^{-1})^{-1} \sum_{0 < \omega_n < \omega_{\mathrm{cut}}} \mathrm{Re}\langle \Delta\phi f^{\dagger} + \Delta^*\phi^* f\rangle$$

$$- 2 \sum_{0 < \omega_n < \omega_{\mathrm{cut}}} \Big(\mathrm{Re}\left\langle \frac{\Delta\phi f^{\dagger} + \Delta^*\phi^* f}{g+1}\right\rangle + 2\omega_n\mathrm{Re}\langle g-1\rangle\Big)\Big\} \tag{10}$$

in our dimensionless unit. S_n is the entropy in the normal state. We calculate $S_s(T)$ numerically using selfconsistent solutions of quasiclassical Green's functions, $\Delta(\mathbf{r})$ and $\mathbf{A}(\mathbf{r})$. By numerical derivative of $S_s(T)$, we obtain the specific heat C as

$$C = T\frac{\partial S_s}{\partial T}. \tag{11}$$

3. Stable Vortex Lattice Configuration When $H \parallel ab$

When $\mathbf{H} \parallel ab$, in the absence of paramagnetic effect ($\mu = 0$), the upper critical field H_{c2} has field orientation dependence; $H_{c2} \sim 1.55$ for $\mathbf{H} \parallel$ antinode and $H_{c2} \sim 1.45$ for
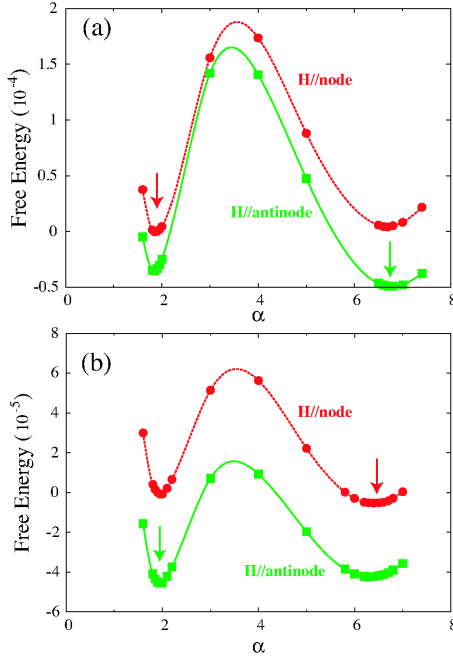
Fig. 3.   (Color online) Free energy $F - F_0$ as a function of α at $T/T_c = 0.1$ (a) and 0.6 (b) in the presence of strong paramagnetic effect ($\mu = 2$). $H/H_{c2} = 0.211$. $F_0 \equiv F(\alpha = 1.9, H \parallel \text{node})$. In each figure, the upper (lower) line shows the case when magnetic field is applied to the node (antinode) direction of the d-wave pairing gap function. For each field orientation, the arrow indicates the minimum of F.

$H \parallel$ node in our parameters. In the case of strong paramagnetic effect $\mu = 2$, H_{c2} is largely suppressed to $H_{c2} \sim 0.190$ both for $H \parallel$ antinode and $H \parallel$ node. There orientation-dependence of H_{c2} becomes isotropic within the ab plane.

First, we discuss the vortex lattice configuration, when magnetic fields are applied parallel to the ab plane, i.e., $H \parallel ab$. In these field orientations, there are two candidates for the stable vortex lattice configuration. One is when one of the neighbor six vortices is located in the ab-direction, as shown in Fig. 2 (a), which is called type-A configuration in this paper. In the other configuration, one of the neighbor vortices is located in the c direction, as shown in Fig. 2 (b), called type-B configuration. In the isotropic case of the s-wave pairing and the Fermi sphere, anisotropy ratio of the vortex lattice defined by $\alpha = 2a_y/\sqrt{3}a_x$ is $\alpha = 1$ in type-A, and $\alpha = 3$ in type-B. In our parameter where anisotropic ratio of Fermi velocity, $\gamma^{-1} \sim 2$, the triangular lattice is distorted by this ratio so that α for stable vortex lattice becomes about two times larger, i.e., $\alpha \sim 2$ or 6. The exact value of α is not trivial because of the contributions of rippled cylindrical Fermi surface and line nodes of d-wave pairing. Thus, we have to estimate α for stable vortex lattice configuration.

In Fig. 3, we plot the free energy F as a function of α for two magnetic field orientations at $T/T_c = 0.1$ and 0.6 in the presence of large paramagnetic effect ($\mu = 2$). There, the local minimum for F is located at two configurations $\alpha \sim 1.9$ (type-A) and 6.6 (type-B). Among two local minima, vortex lattice configuration with lower F is stable, and the other is metastable. When the field is applied to the node direction of the d-wave pairing function, stable vortex lattice is type-A at $T/T_c = 0.1$, and changed to type-B at $T/T_c = 0.6$. On the other hand, when the field is parallel to antinode direction,
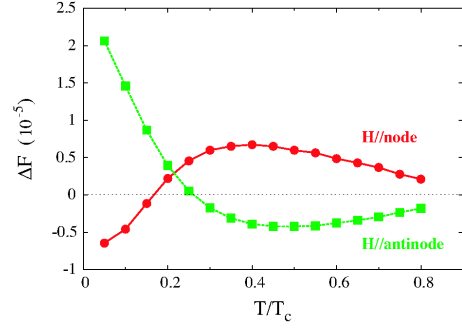

Fig. 4.   (Color online) Temperature-dependence of the free energy difference ΔF between two vortex lattice configurations type-A and type-B. We plot $\Delta F \equiv F(\alpha = 1.9) - F(\alpha = 6.6)$, as a function of T, for two magnetic field orientations $H \parallel$ antinode (squares) and $H \parallel$ node (circles). $\mu = 2$ and $H/H_{c2} = 0.211$.

stable vortex lattice is type-B at $T/T_c = 0.1$, and changed to type-A at $T/T_c = 0.6$. Therefore, the vortex lattice configuration can be changed between type-A and type-B, as a first order transition by rotation magnetic field orientation within the ab plane.

To see the temperature dependence, in Fig. 4 we show the free energy difference ΔF between vortex lattice configurations type-A ($\alpha = 1.9$) and type-B ($\alpha = 6.6$). When $\Delta F > 0$, type-B is stable, and when $\Delta F < 0$, type-A is stable. From Fig. 4, we see that stable vortex lattice configuration is changed at $T \sim 0.2T_c$. Near $T \sim 0.2T_c$ vortex lattice configuration of type-B is stable both field orientations $H \parallel$ node and $H \parallel$ antinode. As seen in Fig. 3, at lower (higher) temperature regions stable vortex lattice configuration is type-A (type-B) for $H \parallel$ node, while the configuration of type-B (type-A) is stable for $H \parallel$ antinode. Thus, the transition of vortex lattice between type-A and type-B can occur upon changing temperature.

For reference, in Fig. 5, we show the results when the paramagnetic effect is absent ($\mu = 0$). There, the results are qualitatively unchanged from those of Figs. 3 and 4 in the strong paramagnetic case. The free energy as a function of α has local minimum at $\alpha \sim 1.9$ and $\alpha \sim 6.6$. At lower T, the stable vortex lattice configuration is type-A for $H \parallel$ node, and type-B for $H \parallel$ antinode. These are changed at higher T.

The purpose of this section was that we proposed the possibility of interesting transitions in the stable vortex lattice configuration when magnetic field is applied to the ab plane. The vortex lattice configuration can be changed between type-A and type-B, depending on T, H, and the field orientation relative to the node direction of the d-wave pairing.[53] It is noted that the results of the stable vortex lattice shown in our calculation is an example for the transition of the vortex lattice configuration. It is not sure that these results of T-dependence are universal. Since the free energy difference ΔF is very small, it is difficult to identify the reason for changes of stable vortex lattice configurations. Detailed forms of Fermi surface shape and anisotropic pairing gap function may change the results for the stable vortex lattice configuration. Therefore, we have to carefully estimate it, using realistic Fermi surface, to compare with future experimental data. However, it is interesting to experimentally identify the phase diagram of the stable vortex lattice configuration under parallel field to the ab plane.
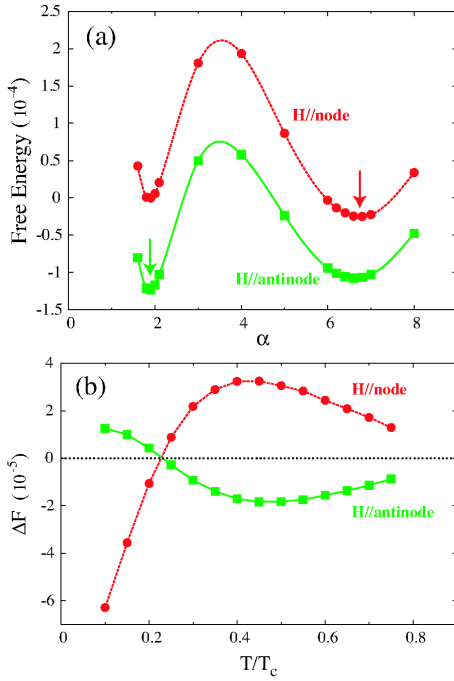
Fig. 5.　(Color online) (a) Free energy $F - F_0$ as a function of α at $T/T_c = 0.6$. $F_0 \equiv F(\alpha = 1.9, H \parallel \text{node})$. For each field orientation, the arrow indicates the minimum of F. (b) T-dependence of the free energy difference $\Delta F \equiv F(\alpha = 1.9) - F(\alpha = 6.6)$, between two vortex lattice configurations type-A and type-B. Here we show the cases without paramagnetic effect ($\mu = 0$) for magnetic field orientations $\mathbf{H} \parallel$ antinode (squares) and $\mathbf{H} \parallel$ node (circles). $H/H_{c2} \sim 0.065$ with $H_{c2} \equiv H_{c2,\text{antinode}} \sim 1.55$.
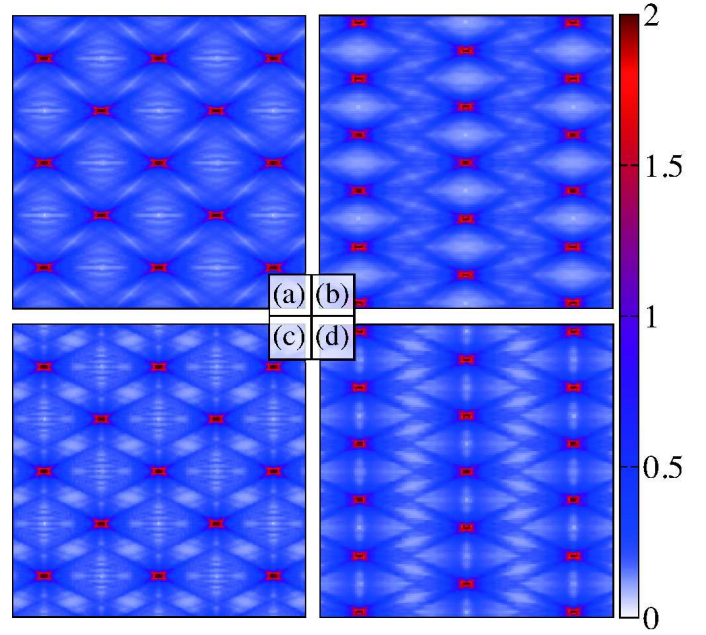

Fig. 6.　(Color online) Spatial structure of zero-energy LDOS $N(E = 0, \mathbf{r})$ for $\mu = 0$ at $H/H_{c2} = 0.065$ in the vortex lattice under magnetic fields parallel to the ab plane. Upper two panels (a) and (b) are for a magnetic field along the antinode direction of the d-wave paring gap function. The vertical axes are [001] directions and the horizontal axes are [100] directions. Lower two panels (c) and (d) are for the node-direction. The vertical axes are [001] directions and the horizontal axes are [110] directions. Left-side two panels (a) and (c) are for the vortex lattice configuration of type-A ($\alpha = 1.9$). Right-side two panels (b) and (d) are for type-B configuration ($\alpha = 6.6$). The view ranges of all four panels are 15×15 in the Eilenberger length unit R_0.

4.　Electronic States in Vortex Lattice When H ∥ *ab*

When we calculate the electronic states, we solve eq. (1) with $i\omega_n \to E + i\eta$. The LDOS is given by $N(\mathbf{r}, E) = N_\uparrow(\mathbf{r}, E) + N_\downarrow(\mathbf{r}, E)$, where

$$N_\sigma(\mathbf{r}, E) = N_0 \langle \text{Re}\{g(\omega_n + i\sigma\mu B, \mathbf{k}, \mathbf{r})|_{i\omega_n \to E + i\eta}\}\rangle_\mathbf{k} \quad (12)$$

with $\sigma = 1$ (-1) for up (down) spin component. We typically use $\eta = 0.01$. The DOS is obtained by the spatial average of the LDOS as $N(E) = N_\uparrow(E) + N_\downarrow(E) = \langle N(\mathbf{r}, E)\rangle_\mathbf{r}$.

To show the electronic states in the vortex lattice for $\mathbf{H} \parallel ab$ without the paramagnetic effect, in Fig. 6 we present zero-energy LDOS $N(\mathbf{r}, E = 0)$ for two vortex lattice configurations type-A and type-B for two magnetic field orientations $\mathbf{H} \parallel$ node and $\mathbf{H} \parallel$ antinode. There, zero-energy electronic states localized around vortex cores have tails extending outside the core. In our calculation, since we assume an open Fermi surface of rippled cylinder, there are not Fermi velocity pointing to the c-axis directions. Therefore quasiparticles with the ab-direction component Fermi velocity dominantly contribute to the zero-energy LDOS. Therefore, $N(\mathbf{r}, E = 0)$ extends to ab direction from vortex cores, reflecting the rippled open Fermi surface. And the connection of zero-energy electronic states between vortices are week along the c-axis direction, compared to other directions. Two parallel lines of the LDOS tails connecting neighbor vortices are due to the interference between electrons at neighbor vortex cores. When zero-energy LDOS are connected between the vortices, the LDOS is suppressed just on the straight line directly connecting the vortex centers, resulting in two parallel tails of zero-energy LDOS.[47] As for the difference between $\mathbf{H} \parallel$ node

and $\mathbf{H} \parallel$ antinode, zero-energy states around vortex core are broadly extended towards outside when $\mathbf{H} \parallel$ node, because superconducting gap has node when quasi-particles propagate to the direction perpendicular to the magnetic field orientation. Zero energy LDOS in the presence of strong paramagnetic effect ($\mu = 2$) is presented in Fig. 7. Due to the Zeeman splitting by strong paramagnetic effect, the original zero-energy bound state for $\mu = 0$ is lifted to finite energy.[43] Thus, the tails extending from vortex cores are smeared in zero-energy LDOS of Fig. 7.

5.　Field-Angle Dependence of Specific Heat

Using selfconsistent results of $\Delta(\mathbf{r})$, $\mathbf{A}(\mathbf{r})$ and quasiclassical Green's functions, we calculate the entropy $S_s(T)$ by eq. (10). In Fig. 8, we show T-dependence of $S_s(T)$. From the T-dependence, we numerically obtain T-dependence of the specific heat by eq. (11), which is presented in Fig. 9. There, $C \propto T^2$ at low fields because of line nodes in the d-wave pairing. As shown in Fig. 9(a) when paramagnetic effect is negligible ($\mu = 0$), with increasing H, C reduces to T-linear behavior due to low energy excitations around vortices, and approaches the line for the normal states. Since T_c decreases with increasing H, the jump of C at T_c becomes smaller at high fields. When paramagnetic effect is strong ($\mu = 2$) as shown in Fig. 9(b), C does not deviate from the low field curve even at $H/H_{c2} = 0.42$, because $H(= 0.08)$ is still small. It changes to the normal state by the first order transition at H_{c2}.
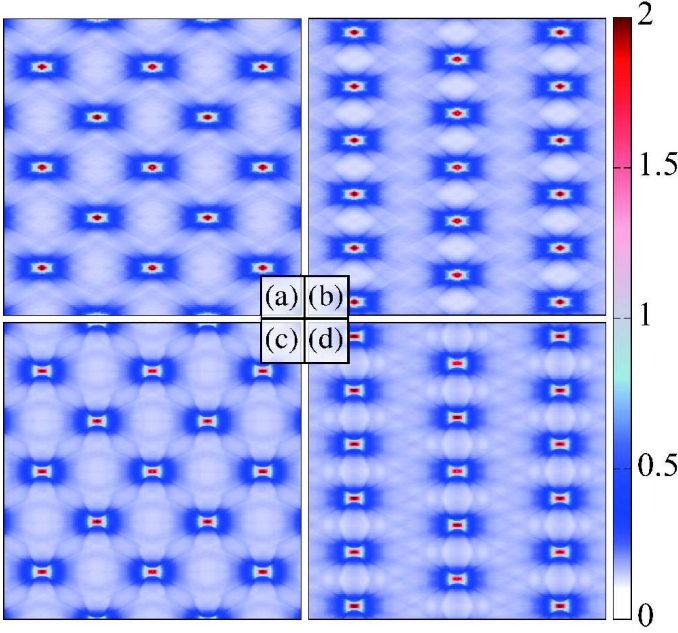
Fig. 7. (Color online) The same as in Fig. 6, but in the presence of strong paramagnetic effect ($\mu = 2$) and $H/H_{c2} = 0.211$. The view ranges of all four panels are 25×25 in the Eilenberger length unit R_0.
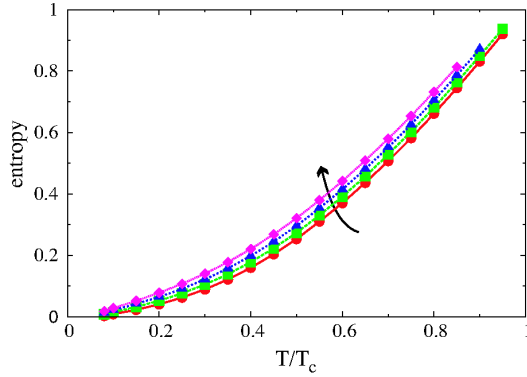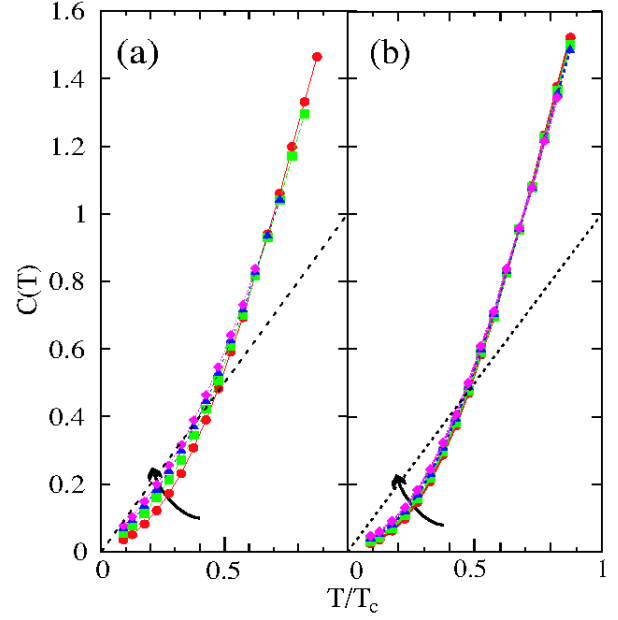

Fig. 9. (Color online) T-dependence of Specific heat C at H/H_{c2} =0.065, 0.194, 0.323, and 0.452 from bottom to top for $\mu = 0$ (a), and at H/H_{c2} =0.105, 0.211, 0.316, and 0.421 from bottom to top for $\mu = 2$ (b). Dotted line indicates $C(T)$ in the normal state.
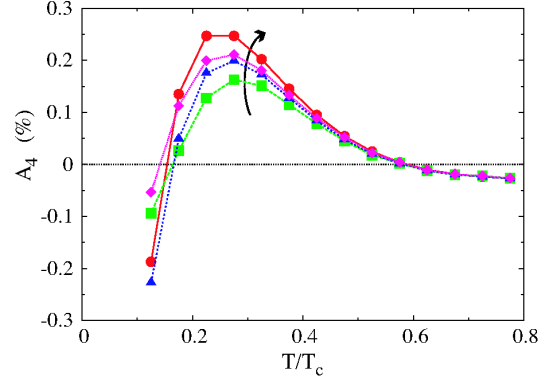

Fig. 8. (Color online) T-dependence of entropy $S_s(T)/S_n(T_c)$ at H/H_{c2} =0.105, 0.211, 0.316, and 0.421 from bottom to top. $\mu = 2$.

Fig. 10. (Color online) T-dependence of fourfold oscillation part A_4 in specific heat under magnetic field rotation at $\mu = 2$ and $H/H_{c2} = 0.211$. We show A_4 for some vortex lattice configurations $(\alpha_{node}, \alpha_{antinode})$ =(6.6,6.6), (1.9,6.6), (6.6,1.9), (1.9,1.9) from bottom to top.

Next, we discuss the oscillation of the specific heat in the form

$$C = C_H(1 - A_4 \cos 4\theta), \qquad (13)$$

when magnetic field orientation is rotated within *ab*-plane. θ is a relative angle between field orientation and antinode-direction of the *d*-wave gap function. The oscillation factor A_4 is calculated by

$$A_4 = \frac{C_{node} - C_{antinode}}{C_{node} + C_{antinode}} \times 100 \; [\%], \qquad (14)$$

where C_{node} ($C_{antinode}$) is the specific heat for field orientation along the node (antinode) direction, i.e., $\theta = 45°$ ($0°$) in the $d_{x^2-y^2}$-wave pairing.

To evaluate how A_4 depends on the vortex lattice configurations type-A and type-B, in Fig. 10 we present T-dependence of A_4 for some choices $(\alpha_{node}, \alpha_{antinode}) = (1.9,1.9)$, (6.6,6.6), (1.9,6.6), (6.6,1.9). α_{node} ($\alpha_{antinode}$) is value of α for vortex

lattice configuration when field orientation is along the node (antinode) direction. From the figure, we see that the choice of the stable vortex lattice configuration does not seriously affect on the behavior of A_4. In any cases, on lowering T from high temperature, A_4 increases with sign change from negative to positive, and after peak near $T \sim 0.3T_c$, A_4 rapidly decreases with sign change to negative. Therefore, we fix the vortex lattice configuration as type-A with $\alpha = 2$, hereafter. We note that C_4 for $\alpha = 2$ does not seriously change from that for $\alpha = 1.9$.

Figure 11(a) shows T-dependence of A_4 for some H. There, for lower H, sign change of A_4 occurs at $T \sim 0.15T_c$. However, at higher H, A_4 remains positive and increases on lowering T. To show the H- and T-dependence, we show contour plot of $A_4(T, H)$ in Fig. 11(b). There solid line indicate
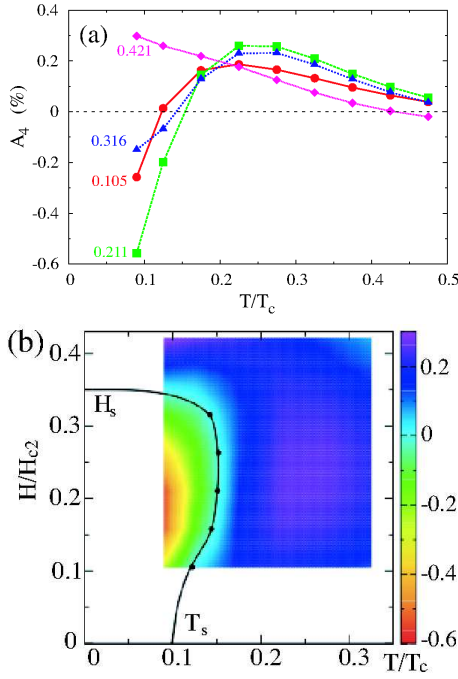
Fig. 11. (Color online) Fourfold oscillation part A_4 of specific heat in the case of strong paramagnetic effect $\mu = 2$. (a) T-dependence of oscillation part A_4 at $H/H_{c2} = 0.105$, 0.211, 0.316, and 0.421. (b) (T, H)-dependence of A_4. The solid curve indicate position of $A_4 = 0$ where sign of the oscillation changes. $H_{c2} \sim 0.19$. $\beta = 0$.
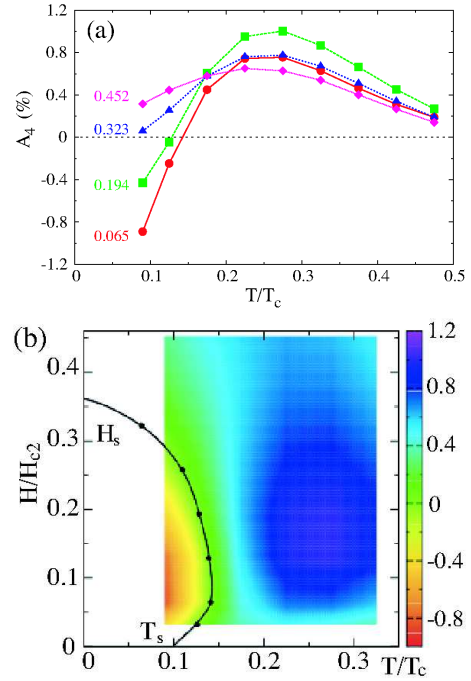
Fig. 12. (Color online) The same as Fig. 11, but in the case when the paramagnetic effect is absent ($\mu = 0$). In (a), $H/H_{c2} = 0.065$, 0.194, 0.323, and 0.452. $H_{c2} \equiv H_{c2,\text{antinode}} \sim 1.55$. $\beta = 0$.

the sign change of $A_4(T, H)$. Inside region from the solid line at lower T and lower H has negative A_4. Other higher T region has positive A_4. We defined the magnetic field where the sign change occurs at low temperature as H_s, and the temperature of the sign change as T_s. In Fig. 11(b) in the presence of strong paramagnetic effect, $T_s/T_c \sim 0.1$ and $H_s/H_{c2} \sim 0.35$ [$H_s \sim 0.067$].

To evaluate the contribution of Pauli-paramagnetic effect, in Fig. 12 we show $A_4(T, H)$ in the case without paramagnetic effect ($\mu = 0$). There, sign change of A_4 similarly occurs at low T and H, while amplitude of A_4 is enhanced compared with that for $\mu = 2$ in Fig. 11. This case ($\mu = 0$) corresponds to the previous work in ref. 27. Our results are qualitatively consistent to it, while we perform selfconsistent calculation without using Pesch approximation. Quantitatively, $H_s/H_{c2} \sim 0.35$ in our calculation becomes smaller than $H_s/H_{c2} \sim 0.5$ in ref. 27. T_s/T_c is almost same in both calculations. The reason of the sign change is because of the E-dependence of DOS $N(E)$, as discussed in ref. 27. Compared with $N(E)$ for $\mathbf{H} \parallel$ node, $N(E)$ for $\mathbf{H} \parallel$ antinode is smaller at low E, but larger at higher E.

Our new approach is to evaluate the contribution of paramagnetic effect, by comparing results in Figs. 11 and 12. By the paramagnetic effect, the upper critical field is largely suppressed from $H_{c2} \sim 1.55$ (when $\mu = 0$) to $H_{c2} \sim 0.19$ (when $\mu = 2$), and the sign change field is also largely suppressed from $H_s \sim 0.54$ to $H_s \sim 0.067$. Thus, in the scale H/H_{c2}, the normalized sign-change field H_s/H_{c2} keeps similar value, which is not seriously changed by the paramagnetic effect. We see also the difference at $H > H_s$, in Fig. 11, A_4 monotonically increase on low temperature, but in Fig. 12, A_4 decreases at low temperature after increase at high temperature.

Thus, solid line of H_s almost horizontal at low T in Fig. 11(b), but the line of H_s increases on lowering T in Fig. 12(b).

Lastly, we also evaluate the contribution of Fermi velocity anisotropy on A_4, considering finite β in the definition of Fermi surface in eq. (2). Figure 13 shows $A_4(T, H)$ for $\beta = 0.5$ and $\mu = 2$. This positive β shifts H_s smaller to $H_s/H_{c2} \sim 0.3$ for $\beta = 0.5$, from $H_s/H_{c2} = 0.35$ for $\beta = 0$ [Fig. 11]. On the other hand, negative β makes H_s larger. Therefore, anisotropic Fermi velocity affect on the sign-change field H_s. However, from Figs. 11 - 13, we see that the sign-change temperature T_s of A_4 is rather independent from the Fermi surface anisotropy and paramagnetic effect.

Recently the sign-change of A_4 in specific heat oscillation was observe in CeCoIn$_5$.[15] There, A_4 shows the sign change at low T and low H. This is qualitatively consistent to our results of calculations, and supports the $d_{x^2-y^2}$-wave pairing for superconductivity in CeCoIn$_5$. Compared to the experimental data in ref. 15, amplitude of A_4 is smaller in our calculation. One of the reason is that in analysis of experimental data definition of A_4 is $C = C_0 + C_H(1 - A_4 \cos 4\theta)$, while in our calculation $C_0 = 0$ in the clean limit. While $T_s/T_c \sim 0.1$ both for experiment and theory, $H_s/H_{c2} \sim 0.1$ in experimental data is smaller than the theoretical calculation. We showed that H_s/H_{c2} can be changed by the Fermi velocity anisotropy, based on a simple β-model. Therefore, as a possibility, by theoretical estimate using realistic Fermi surface structure may improve quantitative accordance of H_s with experimental data.

6. Summary and Discussions

We investigated the vortex state in $d_{x^2-y^2}$-wave pairing when magnetic field $\mathbf{H}$ is applied parallel to ab plane, based on quantitative calculation by selfconsistent Eilenberger the-
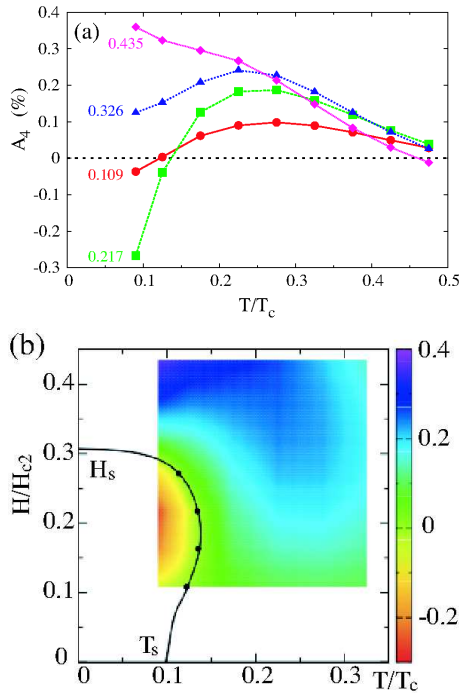
Fig. 13.   (Color online) The same as Fig. 11, but in the case when we include the contribution from anisotropic Fermi velocity by $\beta = 0.5$ with strong paramagnetic effect $\mu = 2$. In (a), H/H_{c2} =0.109, 0.217, 0.326, and 0.435. $H_{c2} \sim 0.184$.

ory. Evaluating (1) stable vortex lattice structure, (2) the zero-energy LDOS in the vortex lattice state, and (3) temperature dependence of specific heat, we estimate the differences of vortex states for **H** ∥ node and for **H** ∥ antinode.

(1) The transition of two possible vortex lattice configurations (type-A and type-B in Fig. 2) can occur as a function of temperature and magnetic field. There is a possibility that vortex lattice configuration for **H** ∥ antinode is different from that for **H** ∥ node. This indicate that by rotation of magnetic field orientation within *ab* plane, first order transition occurs between two vortex lattice configuration.

(2) The spatial structure of zero-energy LDOS reflects Q2D Fermi surface structure. The tails of zero-energy LDOS prefer connecting with those of neighbor vortices in the *ab* direction compared to those in *c* direction. The dependence on the relative angle between the node-direction and magnetic field orientation gives minor contribution to broad extension of quasiparticles around vortex cores.

(3) We evaluated magnetic field and temperature dependence of the amplitude and sign for specific heat oscillation by rotation of magnetic field orientation. The sign of the oscillation changes at low field and low temperature region, where the sign is consistent to the oscillation of evaluation by zero-energy DOS. This sign-change behavior was recently observed in CeCoIn$_5$.[15] Our selfconsistent calculation without Pesch approximation gives qualitatively consistent results to those in previous work by Pesch approximation when the paramagnetic effect is absent.[27] We extend this calculation to the case of strong paramagnetic effect such as CeCoIn$_5$, and show the sign-change behavior of the specific heat oscillation is similar to that without paramagnetic effect, if the magnetic field is scaled by suppressed H_{c2}. We also evaluate the contribution of anisotropic Fermi velocity, which shifts the sign-change field.

The experiments to observe the dependence on magnetic field orientation are useful method to identify the position of the node in the superconducting gap on the Fermi surface. In addition to specific heat oscillation by rotation of magnetic field orientation, we examine the dependence on the relative angle between the node and field orientation for stable vortex lattice configuration and spatial structure of LDOS, with and without paramagnetic effect. The theoretical calculations give valuable information to be compared with details of experimental data.

1) M. Sigrist and K. Ueda: Rev. Mod. Phys. **63** (1991) 239.
2) D. A. Wollman, D. J. Van Harlingen, W. C. Lee, D. M. Ginsberg, and A. J. Leggett: Phys. Rev. Lett. **71** (1993) 2134.
3) C. C. Tsuei, J. R. Kirtley, C. C. Chi, L. S. Yu-Jahnes, A. Gupta, T. Shaw, J. Z. Sun, and M. B. Ketchen: Phys. Rev. Lett. **73** (1994) 593; C. C. Tsuei, J. R. Kirtley, Z. F. Ren, J. H. Wang, H. Raffy, Z. Z. Li: Nature (London) **387** (1997) 481.
4) S. Kashiwaya and Y. Tanaka: Rep. Prog. Phys. **63** (2000) 1641.
5) I. Vekhter, P. J. Hirschfeld, J. P. Carbotte, and E. J. Nicol: Phys. Rev. B **59** (1999) R9023.
6) P. Miranović, N. Nakai, M. Ichioka, and K. Machida: Phys. Rev. B **68** (2003) 052502.
7) P. Miranović, M. Ichioka, K. Machida, and N. Nakai: J. Phys. Condens. Matter **17** (2005) 7971.
8) T. Park, M. B. Salamon, E. M. Choi, H. J. Kim, and S.-I. Lee: Phys. Rev. Lett. **90** (2003) 177001.
9) H. Aoki, T. Sakakibara, H. Shishido, R. Settai, Y. Onuki, P. Miranović, and K. Machida: J. Phys.: Condens. Matter **16** (2004) L13.
10) K. Deguchi, Z. Q. Mao, H. Yaguchi, and Y. Maeno: Phys. Rev. Lett. **92** (2004) 047002.
11) A. Yamada, T. Sakakibara, J. Custers, M. Hedo, Y. Ōnuki, P. Miranović, and K. Machida: J. Phys. Soc. Jpn. **76** (2007) 123704.
12) K. Yano, T. Sakakibara, T. Tayama, M. Yokoyama, H. Amitsuka, Y. Homma, P. Miranović, M. Ichioka, Y. Tsutsumi, and K. Machida: Phys. Rev. Lett. **100** (2008) 017004.
13) T. Park, E. D. Bauer, and J. D. Thompson: Phys. Rev. Lett. **101** (2008) 177002.
14) T. Sakakibara, A. Yamada, J. Custers, K. Yano, T. Tayama, H. Aoki, and K. Machida: J. Phys. Soc. Jpn., **74** (2007) 051004.
15) K. An, T. Sakakibara, R. Settai, Y. Onumi, M. Hiragi, M. Ichioka and K. Machida: Phys. Rev. Lett. **104** (2010) 037004.
16) K. Izawa, H. Yamaguchi, Y. Matsuda, H. Shishido, R. Settai, and Y. Onuki: Phys. Rev. Lett. **87** (2001) 057002.
17) K. M. Suzuki, K. Inoue, P. Miranović, M. Ichioka, and K. Machida: J. Phys. Soc. Jpn. **79** (2010) 013702.
18) H. F. Hess, R. B. Robinson, and J. V. Waszczak: Phys. Rev. Lett. **64** (1990) 2711.
19) N. Hayashi, M. Ichioka, and K. Machida: Phys. Rev. Lett. **77** (1996) 4074.
20) G. E. Volovik: Pis'ma Zh. Eksp. Teor. Fiz. **58** (1993) 457 [JETP Lett. 58 (1993) 469].
21) A. D. Bianchi, M. Kenzelmann, L. DeBeer-Schmitt, J. S. White, E. M. Forgan, J. Mesot, M. Zolliker, J. Kohlbrecher, R. Movshovich, E. D. Bauer, J. L. Sarrao, Z. Fisk, C. Petrovic, and M. R. Eskildsen: Science **319** (2008) 177.
22) S. Ohira-Kawamura, H. Shishido, H. Kawano-Furukawa, B. Lake, A. Wiedenmann, K. Kiefer, T. Shibauchi, and Y. Matsuda: J. Phys. Soc. Jpn. **77**, 023702 (2008).
23) N. Hiasa and R. Ikeda: Phys. Rev. Lett. **101** (2008) 027001.
24) W. K. Park, J. L. Sarrao, J. D. Thompson, and L. H. Greene: Phys. Rev. Lett. **100** (2008) 177001.

25) C. Stock, C. Broholm, J. Huidis, H. J. Kang, and C. Petrovic: Phys. Rev. Lett. **100** (2008) 087001.

26) I. Eremin, G. Zwicknagl, P. Thalmeier, and P. Fulde: Phys. Rev. Lett. **101** (2008) 187001.

27) A. B. Vorontsov and I. Vekhter: Phys. Rev. B **75** (2007) 224501.

28) G. R. Boyd, P. J. Hirschfeld, I. Vekhter, and A. B. Vorontsov: Phys. Rev. B **79** (2009) 064525.

29) A. Bianchi, R. Movshovich, N. Oeschler, P. Gegenwart, F. Steglich, J. D. Thompson, P. G. Pagliuso, and J. L. Sarrao: Phys. Rev. Lett. **89** (2002) 137002.

30) T. Tayama, A. Harita, T. Sakakibara, Y. Haga, H. Shishido, R. Settai, and Y. Onuki: Phys. Rev. B **65** (2002) 180504(R).

31) P. Fulde and R. A. Ferrell: Phys. Rev. **135** (1964) A550.

32) A. I. Larkin and Y. N. Ovchinnikov: Sov. Phys. JETP **20** (1965) 762.

33) A. Bianchi, R. Movshovich, C. Capan, P. G. Pagliuso, and J. L. Sarrao: Phys. Rev. Lett. **91** (2003) 187004.

34) H. A. Radovan, N. A. Fortune, T. P. Murphy, S. T. Hannahs, E. C. Palm, S. W. Tozer, and D. Hall: Nature (London) **425** (2003) 51.

35) T. Watanabe, Y. Kasahara, K. Izawa, T. Sakakibara, Y. Matsuda, C. J. van der Beek, T. Hanaguri, H. Shishido, R. Settai, and Y. Onuki: Phys. Rev. B **70** (2004) 020506(R).

36) C. Capan, A. Bianchi, R. Movshovich, A. D. Christianson, A. Malinowski, M. F. Hundley, A. Lacerda, P. G. Pagliuso, and J. L. Sarrao: Phys. Rev. B **70** (2004) 134513.

37) C. Martin, C. C. Agosta, S. W. Tozer, H. A. Radovan, E. C. Palm, T. P. Murphy, and J. L. Sarrao: Phys. Rev. B **71** (2005) 020503(R).

38) K. Kakuyanagi, M. Saitoh, K. Kumagai, S. Takashima, M. Nohara, H. Takagi, and Y. Matsuda: Phys. Rev. Lett. **94** (2005) 047602.

39) K. Kumagai, M. Saitoh, T. Oyaizu, Y. Furukawa, S. Takashima, M. Nohara, H. Takagi, and Y. Matsuda: Phys. Rev. Lett. **97** (2006) 227002.

40) Y. Matsuda and H. Shimahara: J. Phys. Soc. Jpn. **76** (2007) 051005.

41) S. Ikeda, H. Shishido, M. Nakashima, R. Settai, D. Aoki, Y. Haga H. Harima, Y. Aoki, T. Namiki, H. Sato, and Y. Onuki: J. Phys. Soc. Jpn. **70** (2001) 2248.

42) K. Deguchi, S. Yonezawa, S. Nakatsuji, Z. Fisk, and Y. Maeno: J. Magn. Magn. Mater. **310** (2007) 587.

43) M. Ichioka and K. Machida: Phys. Rev. B **76** (2007) 064502.

44) L. DeBeer-Schmitt, C. D. Dewhurst, B. W. Hoogenboom, C. Petrovic, and M. R. Eskildsen: Phys. Rev. Lett. **97** (2006) 127001.

45) G. Eilenberger: Z. Phys. **214** (1968) 195.

46) U. Klein: J. Low Temp. Phys. **69** (1987) 1.

47) M. Ichioka, N. Hayashi, and K. Machida: Phys. Rev. B **55** (1997) 6565.

48) M. Ichioka, A. Hasegawa, and K. Machida: Phys. Rev. B **59** (1999) 184; M. Ichioka, A. Hasegawa, and K. Machida: **59** (1999) 8902.

49) U. Klein, D. Rainer, and H. Shimahara: J. Low Temp. Phys. **118** (2000) 91.

50) K. Watanabe, T. Kita, and M. Arai: Phys. Rev. B **71** (2005) 144515.

51) M. Ichioka, H. Adachi, T. Mizushima, and K. Machida: Phys. Rev. B **76** (2007) 014503.

52) M. Ichioka, K. Machida, N. Nakai, and P. Miranović: Phys. Rev. B **70**, (2004) 144508.

53) J.S. White and E.M. Forgan: private communications.